EFFECTS OF FEED CONCENTRATION AND WATER VAPOR ON CATALYTIC COMBUSTION OF ETHYL ACETATE AND BENZENE IN AIR OVER CR-ZSM-5 CATALYST

AHMAD ZUHAIRI ABDULLAH, NOR SHAMIRA KAMARUDIN, MOHAMAD ZAILANI ABU BAKAR AND SUBHASH BHATIA

School of Chemical Engineering, Engineering Campus,

University Sains Malaysia, Nibong Tebal, 14300

Seberang Perai Selatan, Penang, MALAYSIA.

E-mail: chzuhairi@eng.usm.my

Abstract: Catalytic combustion of ethyl acetate (EAc) and benzene (Bz) over chromium exchanged ZSM-5 (Si/Al=240) is reported. An 11 mm i.d. fixed-bed catalytic reactor, operated at temperatures between 100 °C and 500 °C, and under excess oxygen condition, was used for the catalytic activity measurement. Apparent order of reaction and apparent activation energy were determined by operating the reactor differentially at a gas hourly space velocity (GHSV) of 78,900 h^{-1} and feed concentrations between 3,500 ppm to 17,700 ppm and 3,700 to 12,400 ppm for ethyl acetate and benzene, respectively. Ethyl acetate was more reactive than benzene due to highly reactive carbonyl group in the molecule. The combustion process satisfactorily fitted pseudo first-order kinetics with respect to organic concentration and a zero-order dependence on the oxygen concentration. The presence of water vapor (9,000 ppm) in the feed stream was found to weaken the reactivity of these organics which could also be demonstrated with increases in the activation energy from 23.1 kJ/mole to 37.6 kJ/mole for ethyl acetate and from 27.6 kJ/mole to 46.1 kJ/mole for benzene. Water vapor was found to play a positive role in the formation of carbon dioxide yield in ethyl acetate combustion. Deactivation of catalyst by water appeared to be only temporary and the activity reverted back to its original value once the source of water vapor was removed.

Keywords: *VOCs, Cr-ZSM-5, ethyl acetate, benzene, humidity, kinetics.*

1. INTRODUCTION

Volatile organic compounds (VOCs) are an important class of air pollutants emitted from many industrial processes [1]. For the abatement of VOC emission, catalytic combustion is considered to be an effective way due to its high removal efficiency and low energy requirement [2,3]. There are numerous catalyst systems intensively investigated for this particular application, among which, ZSM-5 zeolite based catalysts stand out owing to its special pore characteristics and high

hydrothermal stability [4,5]. For the active metal component, chromium provides several advantages over conventionally used noble metals by being low cost but is highly active for the combustion process [6].

In the present work, the combustion of benzene and ethyl acetate are comparatively studied. Benzene, the simplest aromatic compound is widely used as a solvent and is a starting material for many industrial chemicals. However, it is also known to be carcinogenic and need to be removed from the industrial air emission [2]. Meanwhile, ethyl acetate is among the common solvent found in many industries such as paint and coating industries. Despite very low toxicity, its high volume emission can contribute to the occurrence of ground level ozone which is detrimental to health, foliage and many construction materials [7]. Differences in the chemical nature of these two VOCs could provide meaningful conclusion if the behavior of the combustion process were compared.

Some reports have been published regarding the kinetics behavior of zeolite-based catalytic system for treating VOC [2,5]. However, the effect of water vapor as co-feed receives little attention despite being demonstrated to bring about significant and mostly negative effect on the combustion process [2,7]. The effect is attributed to competitive adsorption between VOC and water molecules and the magnitude of the effect may vary depending on the nature of organic molecules [8]. Unfortunately, reports on the effect of water molecule on the kinetic behavior are quite scarce.

The development of a suitable kinetic model to represent the combustion of VOC is a rather complex and challenging task as specific catalyst-VOC system could have different kinetic models. It is more complicated when water presents as a co-feed [5]. Therefore, this work is expected to complement the current knowledge regarding the kinetic behavior of the catalytic system. Here, the process was demonstrated using ethyl acetate and benzene as VOC model compounds without and with interference of water vapor in the feed stream. Chromium was selected to be ion-exchanged into ZSM-5 as it was found to be the most active transition metal to materialize VOC combustion [1,4,9]. This result could provide valuable information on a simple but robust model to represent catalytic combustion of VOCs for the purpose of designing a catalytic system to treat VOC-containing air stream.

2. EXPERIMENTATION

2.1 Catalyst Preparation and Characterization

Chromium exchanged ZSM-5 (Si/Al=240) was prepared in two steps. In the first step, ammonium exchange of the zeolite was performed in 2.25 M of NH_4Cl solution at 60°C for 6 h. The metal exchange step was carried out in an acidified (to pH 4) 28.85 mM of aqueous $Cr(NO_3)_3$ solution (concentration targeted at 3 % metal loading) for 6 h, followed by vacuum filtration, drying and calcinations at 500 °C for 6 h. Before used in the reactor, the catalyst was palletized, crushed and sieved to particle sizes between 0.25-0.30 μm. The catalysts samples were then characterized for surface characteristics using Autosorb-1 surface analyzer and for the final metal loading using Shimadzu AA-650 atomic absorption spectroscopy (AAS).

2.2 Catalyst Performance Study

The catalytic activity test was performed in an 11 mm i.d. quartz reactor charging with required amounts of zeolite catalysts (Figure 1). A VOC-laden air stream was generated by bubbling nitrogen gas through a saturator containing desired organic liquids and another nitrogen flow was used to bubble water in order to introduce water vapor into the resultant gas stream. The total flow

rate was fixed at 250 ml/min by a feed of high purity air to give corresponding gas hourly space velocity (GHSV) of 32,000 h^{-1} except for the kinetic study in which the GHSV was maintained at 78,900 h^{-1} to operate the reactor in differential mode. Details of the experimental conditions are given in Table 1. All of the experiments were conducted under oxygen-rich condition to ensure the reaction was not oxygen-limiting. The inlet and outlet gases were analyzed using an off-line Shimadzu GC-8A gas chromatography equipped with a MS 5A and Porapak Q packed columns.

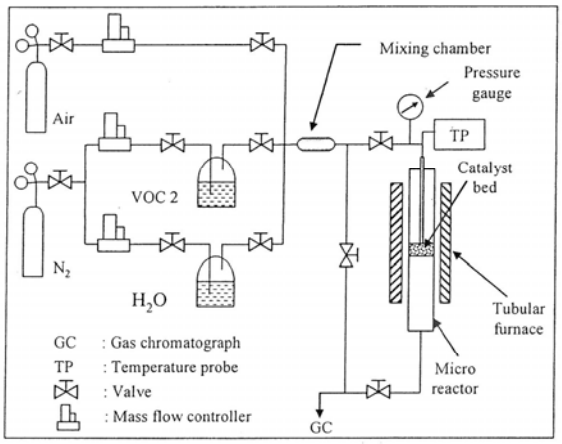

Fig. 1: Experimental set up for the catalyst activity measurement.

Table 1 : Catalytic reactor experimental conditions for ethyl acetate (EAc) and benzene (Bz) conversions.

Reactor Type	GHSV (h^{-1})	W_{cat} (g)	Space Time (s)	Feed O_2 (%)		O_2/VOC ratio	
				EAc	Bz	EAc	Bz
Integral	32,000	0.20	0.113	12.5-19.6	12.5-19.1	11.1-98.0	15.4-95.5
Differential	78,900	0.08	0.046	12.5-19.6	12.5-19.1	11.1-98.0	15.4-95.5

2.3 General Calculations

The VOC removal efficiency, the CO_2 yield and the reaction rate of the reactor were calculated as below:

$$\text{Removal efficiency} = \frac{C_{in} - C_{out}}{C_{in}} \times 100\ \% \quad (1)$$

$$CO_2\ \text{yield} = \frac{F_{CO_2}}{(N)(F_{voc,\,in} - F_{voc,\,out})} \times 100\,\% \quad (2)$$

$$-r_{voc} = \frac{Q}{W}\left(C_{in} - C_{out}\right) \quad (3)$$

where, C_{in} and C_{out} are feed and outlet concentrations (ppm for conversion calculation and mol/ml for reaction rate calculation), respectively, F_x is molar flow rate of component x, N is number of carbon atom in one VOC molecule, $(-r_{voc})$ is the reaction rate of ethyl acetate or benzene (mol/s-g_{cat}) and Q/W is the space velocity (weight hourly in ml/s-g_{cat})

The dependence of the rate of ethyl acetate and benzene combustion on the feed organic concentration and oxygen content was tested using the following simple power-law rate equation.

$$-r_{voc} = kC_{voc}{}^{m}C_{O_2}{}^{n} \quad (4)$$

where, k is the reaction constant, and m and n are reaction orders. Effect of feed oxygen content on the reaction rate was studied by fixed the organic concentration at 2,000 ppm and varying the oxygen content by changing air/nitrogen ratio. Apparent orders of reaction were obtained by plotting $ln(-r_{voc})$ vs $ln(C_{voc})$ at different temperatures and the apparent activation energy (*Eapp*) was calculated as the multiplication product of the slope of the $ln\ k$ vs $(1/T)$ plot and the gas constant (R).

3. RESULTS AND DISCUSSION

3.1 Characteristics of the Catalyst

Table 2 summarizes the characteristics of chromium-exchanged ZSM-5 with its parent zeolite as reference. The data are presented as the mean values of three measurements and their respective standard deviation (mean ± standard deviation). For both materials, the surface area was predominantly contributed by micropores which constituted about 80 % of the total surface area calculated using the Brunneur-Emmett-Teller isotherm (S_{BET}). The ratio between the amount of micropore to mesopore areas was found to be 4.5. Metal exchange process was found to cause about 10 % drop in the S_{BET}. Corresponding reduction in micropore area (significant at 95 % confidence level) was also detected while the effect on mesopore area was minimal. This reduction could be due to the introduction of larger Cr^{3+} cation in place of smaller Na^{+} cation that cost the zeolite some of its micropore area. In addition, partial structural damage and particle agglomeration due to heat treatment used during metal exchange process might be among other causes for the loss of surface area in Cr-ZSM-5 [10].

Table 2 : Characteristic of Cr-exchanged ZSM-5 as compared to its parent H-form.

Catalyst	S_{BET} (m^2/g)	Metal Loading (%)	Pore area		
			Micro (m^2/g)	Meso(m^2/g)	Micro/Meso
H-ZSM-5	393 ± 2	-	321 ± 2	72 ± 2	4.5
Cr-ZSM-5	353 ± 3	0.66 + 0.04	282 ± 1	71 ± 3	4.0

3.2 Effect of Feed Organic Concentration

Figure 2 depicts the conversion and corresponding carbon dioxide yield in the combustion of ethyl acetate and benzene at different feed organic concentrations. It is obvious that ethyl acetate was much more reactive compared to benzene while at the same time, showed better yield towards the production of carbon dioxide as the ultimate oxidation product. It is also worth noting the common trend that, as the feed concentration increased, the conversion and carbon dioxide yield diminished.

Ethyl acetate was more reactive as its molecule had an oxygen-containing group which was a well-known electron-withdrawing group. This made adjacent C–O and C–H bonds more susceptible to breakage. The oxygen atom also had lone pair electrons that could easily interact with vacant *p*-orbital of chromium ion in Cr-ZSM-5 to form active intermediates, leading to the breakage of the molecule [9]. Meanwhile, benzene was less reactive due to occurrence of resonance effect in its ring. Consequently, higher energy was required to cause the extraction of protons which would initiate its combustion. This translated as higher stability of this organic compound towards catalytic combustion.

Low carbon dioxide yield at higher organic reactant concentration was attributed to higher carbon molar flow rate being fed into the reactor. Consequently, some of the products of incomplete combustion would leave the reactor unreacted. In ethyl acetate conversion, acetic acid was identified as the main product of incomplete combustion while for benzene, it was mainly in the form of carbon monoxide.

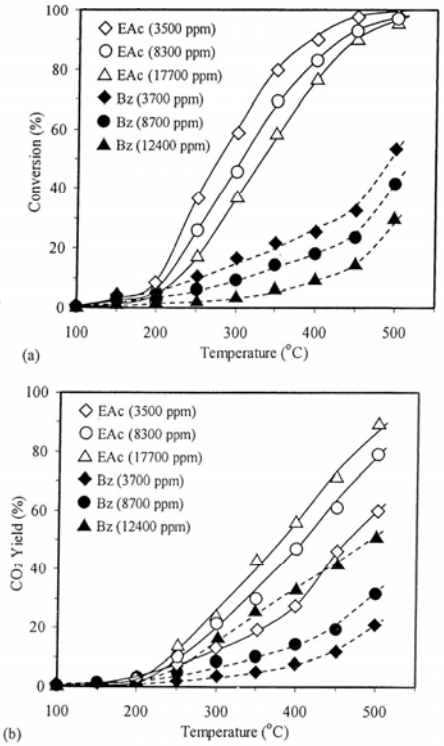

Fig. 2: Profile of ethyl acetate (EAc) and benzene (Bz) conversion (a) and carbon dioxide yield (b) at different feed concentrations (GHSV=32,000 h^{-1}).

3.3 Effect of Water Vapor in the Feed

The presence of water vapor as co-feed was found to negatively affect the conversion of ethyl acetate and benzene as shown in Fig. 3(a). The effect of water vapor was also temperature-dependent as the reduction in conversion decreased with an increase in reaction temperature. One important observation shown in Figure 3(b) is while carbon dioxide yield for benzene combustion was weakened by water vapor, the latter strongly boasted the carbon dioxide formation in the case of ethyl acetate combustion. The magnitude of the effect was also found to increase with an increase in the reaction temperature.

In competitive adsorption of VOC and water, the force of adsorption plays dominant role [7]. Physical adsorption involves interactions of sorbate molecules (VOC and water) with the sorbent (Cr-ZSM-5) which can be accounted for van der Waals forces and electrostatic forces [5]. The magnitude of the forces depends on the polar nature of the sorbate and the sorbent [11]. On polar surfaces, such as cation-exchanged zeolites, electrostatic forces dominated over van der Waals forces. Since water molecule is a polar molecule, the adsorption was favored to consequently cause blockage of cationic sites or salvation of nucleophile, hence, slowed the oxidation of the organic [1]. Water molecules also had cluster-forming ability around active sites, thereby, creating diffusion

block for VOC molecules [12]. At higher temperatures, this localization might be prevented and consequently the deactivation effect by water molecules diminished accordingly as observed in Fig. 3(a).

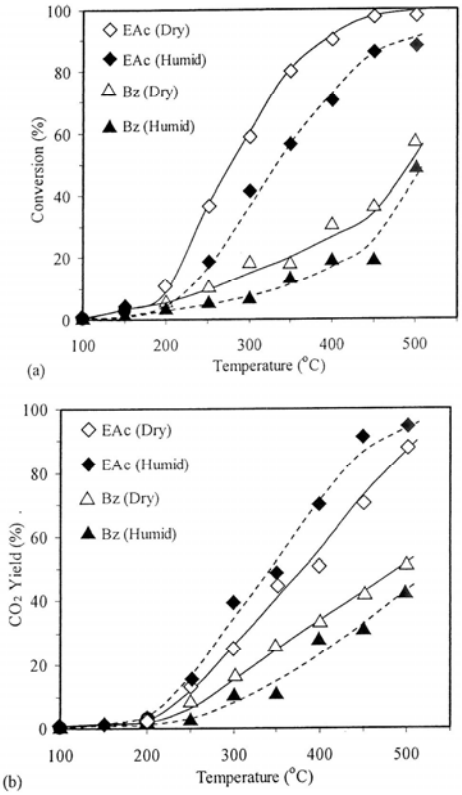

Fig. 3: Profile of ethyl acetate (EAc) and benzene (Bz) conversion (a) and carbon dioxide yield (b) for dry and humid (9,000) feed stream (GHSV=32,000 h^{-1}, C_{voc}=2,000 ppm).

Despite physical blocking of the adsorption of VOC molecules on cationic sites in Cr-ZSM-5, chemically, water molecules might promote the reaction as in the case of ethyl acetate combustion. While water and benzene molecules being absorbed side-by-side, water molecules as electron-rich species might disturb the electronic cloud in ethyl acetate molecules to result in the increase in its reactivity [5]. Consequently, the yield towards carbon dioxide was improved while the fraction of ethyl acetate decomposed decreased as shown in Fig. 3(b).

An experiment was conducted to study the reversibility of water poisoning on the catalytic combustion of ethyl acetate and benzene. Upon the inclusion of 9,000 ppm of water vapor as co-feed, the conversions were found to plunge about 30 % for ethyl acetate and 15 % for benzene (Fig. 4). When the source of water vapor was removed at the end of the second hour on stream, the activity of the catalyst was found to immediately revert back to its original value. This observation suggested only reversible physical interactions involved between water molecule and catalytically

active cationic sites. However, at more extreme conditions of high temperature and humidity and longer time on stream, the possibility of chemical modification of the zeolite catalyst leading to its deactivation could not be ruled out [9].

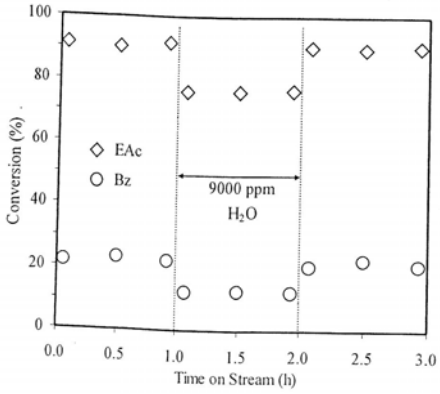

Fig. 4: Reversibility study on the effect of water vapor on ethyl acetate (EAc) and benzene (Bz) conversions (GHSV=32,000 h^{-1}, reaction temperature=400 °C, Cvoc=2,000 ppm).

3.4 Kinetic Study

The kinetic study of ethyl acetate and benzene conversion, with and without the presence of water vapor (9,000 ppm) as co-feed was conducted using the reactor operating in differential mode. The apparent orders of reaction (n_{app}) for reaction carried our at different conditions were calculated from the slope of $ln(-r_{voc})$ vs $ln(C_{voc})$ plots. However, those plots have been excluded to avoid redundancy in the number of figure and the misleading of the overall discussion. This is because it is just a well-known mathematical method used to estimate the values of the parameters (or constants) in any linear equation and not much useful information is expected from the visual analysis of the figures. Moreover, the information of interest from the plot is just the comparison between the values of apparent reaction order (n_{app}), frequency factor (A) and apparent activation energy (E_{app}) and these data are best presented in tabular form as given in Table 3. It is evident in the table that the ethyl acetate and benzene combustion processes approached a pseudo first-order reaction with respect to organic feeds with n_{app} were 0.98 and 0.94, respectively. These values show slightly increase when 9,000 ppm of water vapor present in the feed. A first-order dependence of reaction rate with feed organic concentration was also reported by Lou and Lee [11] using trichloromethane as their VOC model compounds.

Figure 5a and 5b demonstrate the effect of feed oxygen partial pressure on the reaction rate of ethyl acetate and benzene, respectively. According to the results, the reaction rates were strongly temperature-dependent. However, the effect of oxygen partial pressure on the reaction rate was insignificant and could be approximately shown by straight horizontal lines. The dependence of the reaction rate with oxygen concentration in the feed was therefore approximated by a zero-order kinetics. Notably, the feed VOC concentration was significantly more influential than the oxygen concentration. Thus, the reaction rate laws for ethyl acetate and benzene conversions could be expressed by a general equation,

$$-r_{VOC} = kC_{VOC}{}^{1}C_{O_2}{}^{0} \qquad (5)$$

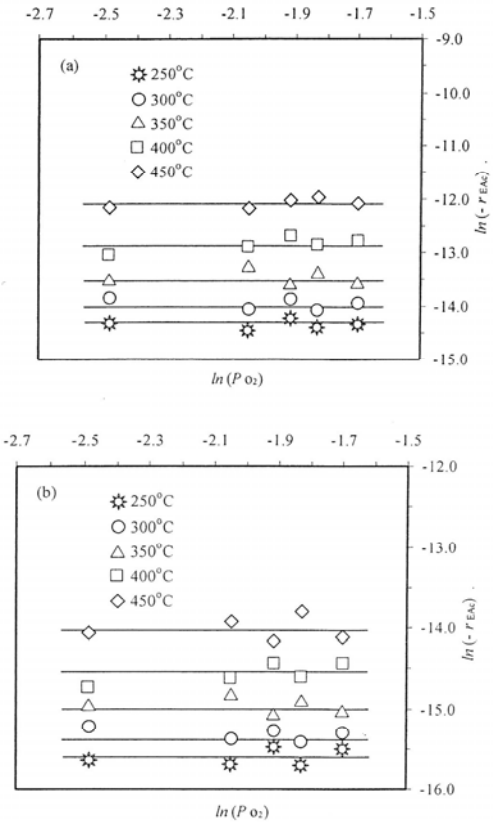

Fig. 5: Dependence of rate of ethyl acetate (EAc) (a) and benzene (Bz) (b) combustion with partial pressure of oxygen in the feed (GHSV=78,900 h^{-1}, C_{VOC}=2,000 ppm).

Table 3: Apparent order of reaction (n_{app}), frequency factor (A) and activation energy (E_{app}) for dry and humid feeds.

VOC	Dry			Humid (9,000 ppm water)		
	n_{app}	$A(s^{-1})$	E_{app} (kJ/mol)	n_{app}	$A(s^{-1})$	E_{app} (kJ/mol)
Ethyl acetate	0.98	$6.39x10^2$	23.1	1.19	$7.38x10^3$	37.6
Benzene	0.94	$2.52x10^2$	27.6	1.10	$3.20x10^3$	46.1

The reaction apparent activation energies (E_{app}) were calculated from the Arrhenius plot (Fig. 6) by assuming first-order reaction with respect to organics feed concentration (or m=1 in Equation

4) and a zero-order with respect to oxygen concentration (or n=0 in Equation 4). In other words, linear relationship between ($-r_{voc}$) and C_{voc} is expected at constant partial pressure of oxygen and ($-r_{voc}$) is independent of C_{O2} at constant C_{voc}. As shown in Table 3, the E_{app} for ethyl acetate is 23.1 kJ/mol while for benzene the value stood at 27.6 kJ/mol. When the catalyst was reversibly deactivated by water molecules, the E_{app} increased to 37.6 kJ/mol and 46.1 kJ/mol, respectively.

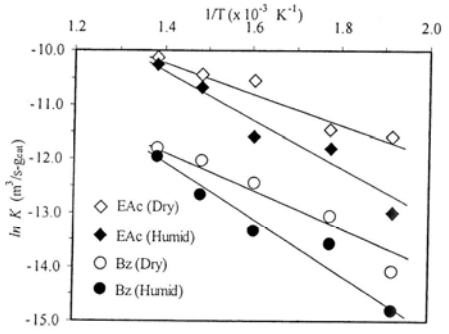

Fig. 6: Arrhenius plot for ethyl acetate (EAc) and benzene (Bz) conversions for dry and humid (9,000 ppm water vapor) feed (GHSV=78,900 h^{-1}).

4. CONCLUSION

Ethyl acetate was significantly more reactive compared to benzene and it is attributed to the presence of highly reactive carbonyl group in ethyl acetate while resonance effect stabilized the benzene molecules. The conversion and the carbon dioxide yield were found to decrease with an increase in reactant concentration. Catalytic combustion of these two organics was demonstrated to approach a pseudo first-order and zero-order kinetics with respect to the feed organics and oxygen concentrations, respectively. Water vapor (9,000 ppm) in the feed stream could retard the combustion of these organics which could also be demonstrated with increases in the activation energy from 23.1 kJ/mol to 37.6 kJ/mol for ethyl acetate and, from 27.6 kJ/mol to 46.2 kJ/mol for benzene. However, water vapor was found to play a positive role in the formation of carbon dioxide in ethyl acetate combustion. Deactivation of the catalyst by water appeared to be only temporary and the activity reverted back to its original value once the source of water vapor was removed.

ACKNOWLEDGEMENT

The authors would like to acknowledge Universiti Sains Malaysia for supporting this work under short term research grant (073518), Ministry of Science, Technology and Innovation of Malaysia (MOSTI) for providing IRPA research grant (08-02-05-1039 EA 001) and the generosity of Süd-Chemie AG Germany for supplying zeolite samples.

REFERENCES

[1] G.A. Atwood, H.L. Greene, P. Chintawar, R. Rachapudi, B. Ramachandran and C.A. Vogel, "Trichloroethylene Sorption and Oxidation Using Dual Function Sorbent/catalyst in a Falling Furnace Reactor", Appl. Catal. B, vol 18, pp 51-61, 1998.

[2] L. Becker, and H. Förster, "Oxidative Decomposition of Benzene and Its Methyl Derivatives Catalyzed by Copper and Palladium Ion-exchanged Y-type Zeolites", Appl. Catal. B, vol 17, pp 43-49, 1998.

[3] P. Dégé, L. Pinard, P. Magnoux, and M. Guisnet, "Catalytic Oxidation of Volatile Organic Compounds II: Influence of Physiochemical Characteristics of Pd/HFAU Catalysts on the Oxidation of o-xylene", Appl. Catal. *B*, vol 27, pp 17-26, 2000.

[4] A.Z. Abdullah, M.Z. Abu Bakar and S. Bhatia, "Coking Characteristics of Chromium-exchanged ZSM-5 in Catalytic Combustion of Ethyl Acetate and Benzene in Air", Ind. Eng. Chem. Res., vol 42, pp 5737-5744, 2003.

[5] A.Z. Abdullah, M.Z. Abu Bakar and S. Bhatia, "A Kinetic Study of Catalytic Combustion of Ethyl Acetate and Benzene in Air Stream Over Cr-ZSM-5 Catalyst", Ind. Eng. Chem. Res., vol 42, pp 6059-6067, 2003.

[6] A.Z. Abdullah, M.Z. Abu Bakar and S. Bhatia, "Performance Study of Modified ZSM-5 as Support for Bimetallic Chromium-copper Catalysts for VOC Combustion", J. Chem. Technol. Biotechnol, vol 79, pp 761-768, 2004.

[7] S. Chatterjee and H.L. Greene, "Oxidative Catalysis of Chlorinated Hydrocarbons by Metal-loadedAcid Catalysts", J. Catal., vol 130, pp 76-85, 1991.

[8] A.Z. Abdullah, M.Z. Abu Bakar and S. Bhatia, "Performance of H-ZSM-5-Supported Bimetallic Catalysts for the Combustion of Polluting Volatile Organic Compounds in Air", J. Chem. Technol. Biotechnol, vol 80, pp 1016-1025, 2005.

[9] P.S. Chintawar, H.L. Greene, "Adsorption and Catalytic Destruction of Trichloroethylene in Hydrophobic Zeolites", Appl. Catal. B, vol 14, pp 34-47, 1997.J.

[10] Weitkamp, S. Ernst and L. Puppe, "Shape-selective Catalysis in Zeolites, in Catalysis and Zeolites : Fundamentals and Applications", edited by J. Weitkamp, and L. Puppe, Springer, Berlin. pp 327-376, 1999.

[11] J.C. Lou and S.S. Lee, "Destruction of Trichloromethane With Catalytic Oxidation", Appl. Catal. B, vol 12 pp 111-123, 1997.

[12] A.Z. Abdullah, M.Z. Abu Bakar and S. Bhatia, "Combustion of Chlorinated Volatile Organic Compounds (VOCs) Using Bimetallic Chromium-copper Supported on Modified H-ZSM-5 Catalyst", J. Hazard. Mater. B, vol 129, pp 39-49, 2006.

A STUDY OF COMPARTMENT FIRE UNDER FORCED VENTILATION: EXPERIMENTAL AND COMPUTATIONAL FLUID DYNAMICS MODELING

M.Z. ABU BAKAR[1] AND Y. WU[2]

[1]*School of Chemical Engineering, Universiti Sains Malaysia,*

Engineering Campus, 14300 Seberang Perai, Penang, MALAYSIA

[2]*University of Sheffield, Department of Chemical Engineering, United Kingdom*

E-mail: chmohdz@eng.usm.my

Abstract: This paper discusses on the dynamic behavior of the flame and smoke inside a compartment fire. The compartment can be referred to a room, road tunnel, duct, compartment or a building. A series of small scales experiments were carried on four rectangular ducts that have the same height (250 mm) but different widths (125 mm, 250 mm, 500 mm and 1000 mm). Fire simulations on the same compartments were performed to investigate the effectiveness of Computational Fluid Dynamics (CFD) in predicting fire phenomenon. CFD was found capable to predict fire phenomenon such as flame shape, flame height and flame tilt angle similar to the experiment.

Keywords: *Smoke flow, fire plume, compartment fire, buoyancy*

1. INTRODUCTION

Fire is an extremely complex phenomenon with various hazards to human, properties and environment. It embraces nearly all the effect found in subsonic chemically reacting flow. Fluid dynamics, combustion, kinetic, radiation and in many cases multi-phase flow effects are linked together to provide the extreme complex physical and chemical phenomenon. It is this complexity that delayed the development of fire research as a science until approximately the 1950s. Due to this complexity, attempts have been made in the mathematical modeling to study, understand and foremost to visualize the basic phenomenon of fire from first principles via solution of the basic conservation equations.

In a typical compartment fire, once the flames have reached the ceiling, they can no longer travel upwards and must therefore travel horizontally. Since they are very hot and therefore light gases, they travel under the ceiling and this situation can elongate as much as 5 – 10 times of an open fire [1]. This elongation arises because the mixing of the air into the flame under the ceiling is by a much slower process than the flame travels vertically. Therefore, in order to entrain enough air to burn all the volatile fuel, the horizontal flame has to be much longer. This phenomenon is shown in Fig. 1a to 1c.

The behavior of a fire in a compartment has been studied by a number of researchers [2-5]. Apart from the dynamic behavior of the fire, the study on the movement of the combustion products such as the smoke has equal importance. This is because smoke is one of the major factors that cause injuries and deaths.

The main objective of this work is to study the dynamic behavior of compartment fire. Parameters such as flame height and flame tilt angles for various fire sizes and ventilation velocities will be investigated by using both experimental and CFD modeling.

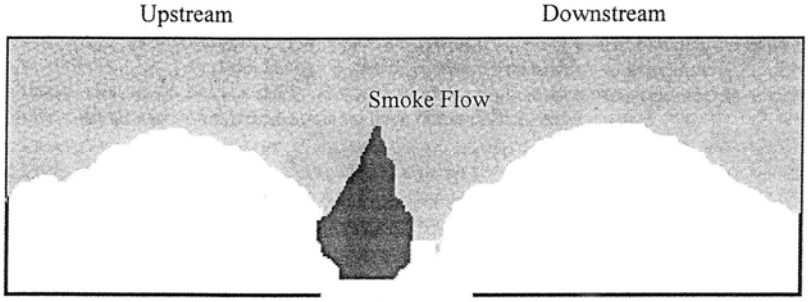

Fig. 1a: Illustration of a compartment fire without ventilation.

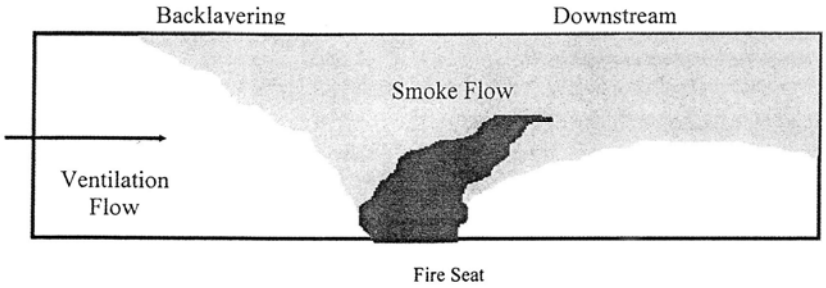

Fig. 1b: Illustration of a compartment fire with low ventilation.

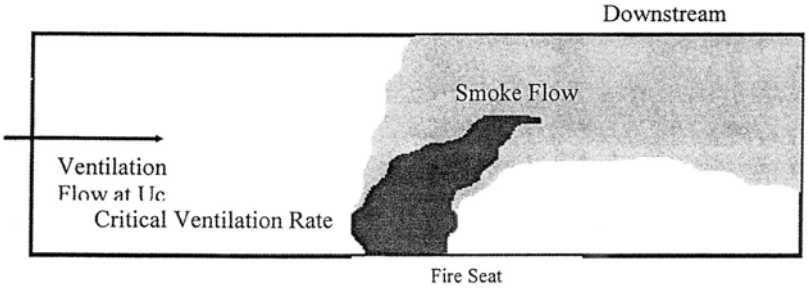

Fig. 1c: Illustration of a compartment fire with critical ventilation.

2. EXPERIMENTAL WORK

The schematic front view and the cross-section of the compartment are shown in Fig. 2. The majority of the model, including the base, was constructed from Perspex (PMMA) of thickness 6.25 mm. To prevent heat damage, the section closet to and downstream of the fire was made from 18 SWG (1.25 mm thick) stainless steel. Additionally, the section closet to the fire was cooled throughout the tests by a water spray. The entire compartment, of approximately 15 m length, was mounted on a series of brackets, which in turn were attached to wall-mounted frames. The height of each compartment was 250 mm and the width varying from 125 mm to 1000 mm.

Propane gas was used as a fuel, metered through a rotameter. This was introduced via a 106 mm diameter porous bed burner with its top surface set flush with the compartment floor. The propane flow rate was varied between 1 and 20 litres per minute, producing fires of 1.4 to 28 kW. These fire sizes correspond to fires of approximately 2.5 to 50 MW in a compartment of diameter around 5 m when the scaling procedure was applied. All products of combustion were exhausted to atmosphere at the downstream end of the compartment.

The ventilation air supply to the compartment was channelled in through a 101.6 mm steel pipe fitted with an orifice plate of throat diameter 71.8 mm, constructed in accordance with BS 1042. The flow was driven by a compressed air. The detailed structure of the air supply system can be found in reference [6]. The orifice plate provides a useful method of determining the total volumetric flow of air. K-type thermocouples were used to measure the temperatures inside the compartment.

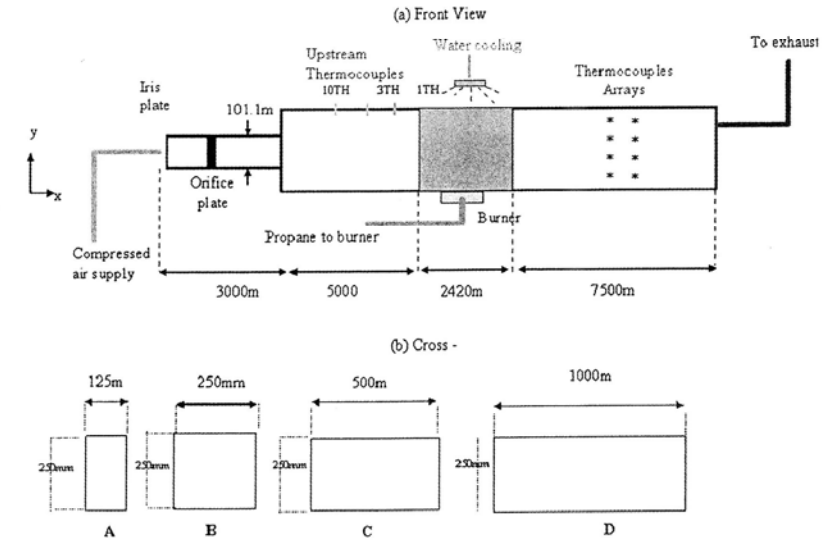

Fig. 2: Schematic front view and cross-section of experimental rig.

3. COMPUTATIONAL FLUID MODELLING

Three-dimensional simulations of smoke flow in the compartments have been carried using Computational Fluid Dynamics software, known as FLUENT. The combustion was considered to be a stoichiometric reaction of propane and air defined as

$$C_3H_8 + 5(O_2) \Rightarrow 3CO_2 + 4H_2O \quad (1)$$

Two combustion models namely, the Magnussen and Hjertager [7] eddy-dissipation model and the mixture fraction/PDF approach have been used to model the combustion process. It was shown that the PDF approach used less CPU time and provides a better prediction of the flame shapes. Therefore most of the CFD simulations were carried out using the PDF approach.

The standard k-ε turbulence model was used to model the flow inside the compartments due to its simplicity and effectiveness. The standard k-ε turbulence model [8] includes basic modifications for buoyancy based on Ljubeja and Rodi [9] in the k-ε equation. The standard k-ε model is a two-equation eddy viscosity turbulence model which transport equations for two variables: k the turbulence energy, and ε the rate of viscous dissipation of turbulence energy. The turbulent effective viscosity, μ_t, is related to k and ε, by a velocity scale ($k^{1/2}$) and a length scale ($k^{3/2}/\varepsilon$) by the expression:

$$\mu_t = \rho C_\mu \frac{k^2}{\varepsilon} \quad (2)$$

and the velocity and length scales are predicted at each point in the flow via the solution of transport equations for k and ε:

$$\frac{\partial}{\partial x_i}(\rho u_i k) = \frac{\partial}{\partial x_i}\left(\frac{\mu_t}{\sigma_k}\frac{\partial k}{\partial x_i}\right) + G_k + G_b - \rho\varepsilon \quad (3)$$

$$\frac{\partial}{\partial x_i}(\rho u_i \varepsilon) = \frac{\partial}{\partial x_i}\left(\frac{\mu_t}{\sigma_\varepsilon}\frac{\partial \varepsilon}{\partial x_i}\right) + C_1\frac{\varepsilon}{k}(G_k + (1 - C_{3\varepsilon})G_b) - C_2\rho\frac{\varepsilon^2}{k} \quad (4)$$

Turbulence is generated according to G_k, where:

$$G_k = \mu_t\left(\frac{\partial u_j}{\partial x_i} + \frac{\partial u_i}{\partial x_j}\right)\frac{\partial u_j}{\partial x_i} \quad (5)$$

and G_b is the generation due to buoyancy:

$$G_b = -g_i\frac{\mu_t}{\rho\sigma_h}\frac{\partial \rho}{\partial x_i} \quad (6)$$

where σ_h is the turbulent Prandtl number, $\frac{\mu_t C_p}{k_t}$.

and $C_{1\varepsilon}$, $C_{2\varepsilon}$, C_{μ}, σ_k and σ_ε are empirical constants, with values, 1.44, 1.92, 0.09, 1.0 and 1.3 respectively. $C_{3\varepsilon}$ is used to take account of the buoyancy effects. Woodburn and Britter [10,11] used $C_{3\varepsilon}$ equal to 0.20 and showed that the inclusion of the modified buoyancy gave better predictions between the measured and predicted results. The present study tested the influence of the value of $C_{3\varepsilon}$ in the prediction of backlayering and found that $C_{3\varepsilon}$ = 0.25 was optimal.

The total simulated compartment length was 8.1 m with the exclusion of a downstream section of 3.0 m length. The longitudinal computational domain was divided into three segments. Segment 1 was the upstream section of 5.0 m length. Segment 2 was the burner section of 0.1 m length and segment 3 was the downstream section of 3.0 m length. The first plane of the longitudinal domain was set to be the inlet of the ventilation flow and the last plane was set as the output of the smoke flow to the exhaust. The wall of the compartment was set to be a solid containing 1 cell. A non-uniform grid distribution was made to avoid a very large number of computational cells, while maintaining a sufficient degree of accuracy in the solution. The longitudinal and vertical grids were set at 102 and 28 cells, respectively. The half cross-sectional cells varying from 8, 14, 28 and 38, dependent on compartment widths. The total cells are, 22 848, 39 984, 79 968 and 10 8528 for the Compartments A, B, C and D, respectively. Grid sensitivity tests have been carried out and the results showed that the grid distributions for the compartments were sufficient.

Figures 3 and 4 show the longitudinal grid distribution for the compartments and the cross-sectional grids for each compartment.

4. RESULTS AND DISCUSSION

(A) EXPERIMENTAL

4.1 Behavior of the Flame

McCaffrey [12] proposed fire plume theory by studying a fire plume above a 30 cm square porous burner. A free fire plume consists of three distinct regimes. The three regimes are:

- Near fire, above the burner, where there is persistent flame and accelerating flow of burning gas
- A region in which there is intermittent flaming and a near-constant flow velocity (intermittent zone)
- The buoyant plume, which is characterised by decreasing velocity and temperature with height.

Figure 5 shows a photograph of a fire in one of the compartment at 15.0 kW. There are two distinguished regions that can be observed; the flame and the buoyant smoke flow. With the presence of longitudinal ventilation flow, the fire plume deflects at certain angle from the vertical. The fire plume still consists of three distinguished regions, similar finding from McCaffrey [12]. The present work considered that the temperature in the persistence flame regime is greater than

500 °C. The temperature in the intermittent regime is between 250 °C to 500 °C. The buoyant plume is considered to have temperature less than 250 °C.

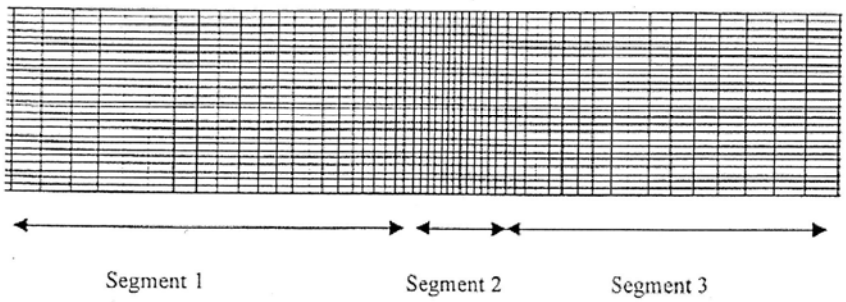

Fig. 3: Longitudinal grid distribution.

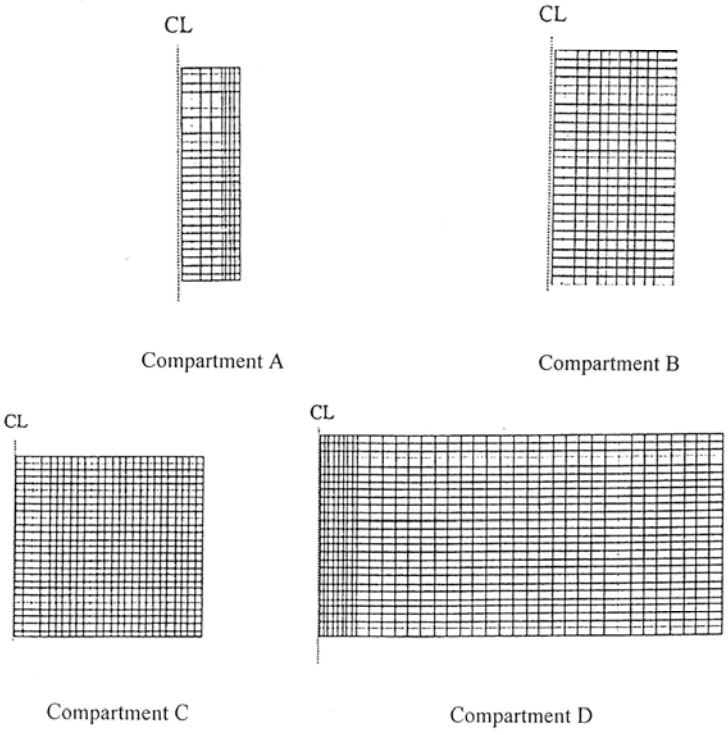

Fig. 4: Cross-sectional grid distribution.

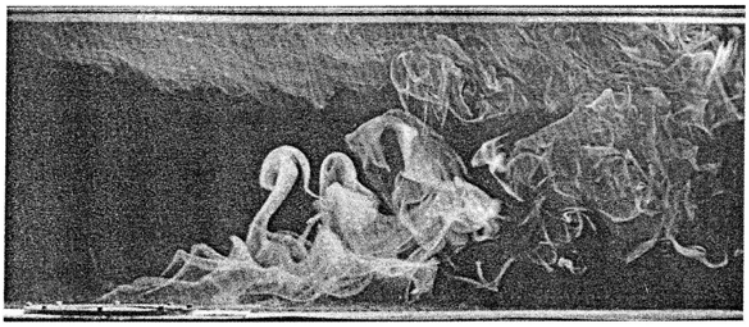

Fig. 5: Photograph of a fire in along compartment.

4.2 Flame Height

Unlike in an open fire, it was observed that the flame heights inside the compartment depend on the interaction between the fire plume with the compartment geometry and the ventilation flow. An attempt was made to illustrate the flame height with two main parameters; the fire sizes and ventilation velocity. Since the exact regimes associated with the fire plume were difficult to determine, both temperature values of 250 °C and 350 °C were selected to justify the boundaries for the intermittent regimes, while the boundary for the persistent regime remains at 500 °C.

Figure 6 depicts the measured temperature contour in compartment B at three fire sizes (3.0kW, 7.5 kW and 15.0kW). It can be observed that as fire size increases, the fire inside the compartment also grows in size. The maximum temperature recorded at 3.0 kW, 7.5 kW and 15.0 kW were in the order of 586 °C, 679 °C and 746 °C, respectively. The results show that for a small fire (3.0 kW), both intermittent regimes indicated by 250 °C and 350 °C is approximately at 125 mm above the compartment floor. Whilst, the persistent regimes in the three compartments lay low. However at 7.50 kW fire, the intermittent regimes indicated by the 250 °C contours have definitely reached the ceiling, while the intermittent regimes indicated by 350 °C have nearly reached the ceiling for all compartments. The persistent flames in the three compartments are approximately at 125 mm above the compartment floor. Finally at 15.0 kW fire, both intermittent regimes have already reached the ceiling, while the persistent flame have not yet reached the ceiling.

4.3 Flame Angle (α)

The measured flame tilt angles from the vertical for three fire sizes at least at two ventilation velocities are shown in Table 1. The tilt angle for 3.0 kW fire at the critical ventilation velocity (0.48 m/s) was 70°. When the fire size was increased to 7.50 kW, the tilt angle at the critical ventilation velocity (0.56 m/s) further increased to 73°. Finally at 15.0 kW, the tilt angle further increased to 76°. A similar pattern occurred in both compartments **A** and **D**. In general, it was found that the deflection angles of the fire plumes in all compartments were greater that 45 °.

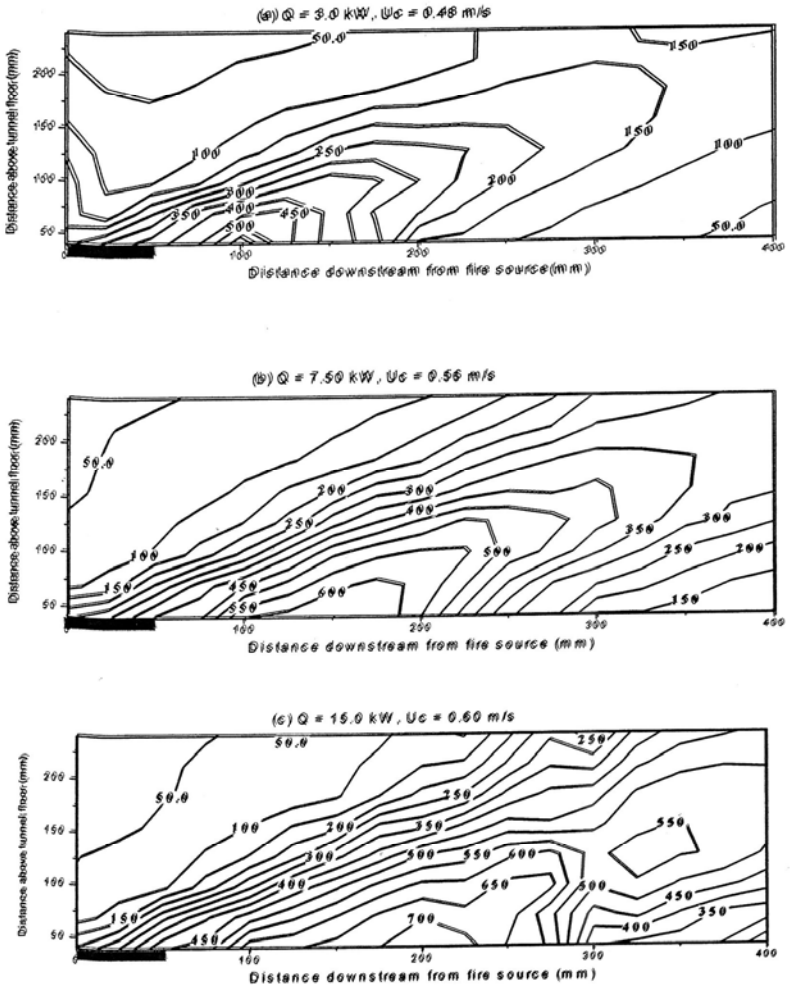

Fig. 6: Measured temperature contours at fire region for 3.0 kW, 7.50 kW, 7.5 kW and 15.0 kW fires.

Table 1: Measured plume tilt angle at various ventilation velocities and fire sizes.

Compartment B			Compartment D			Compartment A		
Q (kW)	V (m/s)	α (°)	Q (kW)	V (m/s)	α (°)	Q (kW)	V (m/s)	α (°)
3.0	0.35	60	3.0	0.18	47	3.0	0.25	65
	0.48	70		0.40	60		0.46	75
	0.96	78		0.50	64			
7.50	0.31	68	7.50	0.28	57	7.50	0.25	70
	0.56	73		0.54	65		0.48	79
15.0	0.34	73	15.0	0.35	60	-	-	-
	0.60	76		0.65	70	-	-	-

(B) COMPUTATIONAL FLUID MODELLING

4.4 Behavior of the Flame

Figure 7a to 7c show the simulated temperature distribution for compartment B at the same fire sizes 3.0 kW, 7.5 kW and 15.0 kW, respectively. With the interaction between compartment geometry and the ventilation flow, the fire plume rises above the compartment floor and deflects at certain angle from the vertical. The sizes and shapes of the fire plume can be clearly seen.

Figure 7 also indicates that CFD simulations predicted a slightly higher temperature in the flame area. The maximum temperature reached approximately 2200 K, which was quite high for propane and air burner combustion. This is caused by the combustion models employed by the FLUENT.

The turbulent combustion models are based on fast chemistry concepts, which overestimates the reaction rates. Therefore, the temperature is over predicted in the flame area. This problem is well known by the CFD simulation community. Both the scientists and CFD commercial users have pointed out the needs of better turbulence models. However, this is not the scope of the present study. Therefore, this problem will not be discussed further.

Another limitation of the combustion models is that the combustion is directly determined by the present of the fuel, therefore the CFD simulation can only predict continuous flame. The intermittent flames existing in the real fire plumes could not be predicted by the CFD simulations.

4.5 Flame Height and Flame Width

Based on the new temperature boundary for each regime as being defined in the previous section, the flame height in each compartment was measured. The results showed that for a small fire (3.0 kW), the intermittent flame was approximately one third of the height of the compartment. For medium size fire (7.50 kW), the intermittent flame was approximately three quarter of the height of the compartment. Finally at higher fire size (15.0 kW), the intermittent flame already reached the compartment ceiling.

The CFD results also showed that the persistent flame never reached the ceiling at critical condition even at higher fire size as shown in Fig. 7 for 15.0 kW fire. The persistent flame (>1500 K) only elongated further downstream. The variations of the flame heights predicted by CFD were almost similar to the experimental results, previously discussed in Section (A).

4.6 Flame Angle (α)

The measured tilt angles of the plume are shown in Table 2. Similar to the experimental results, CFD predicted the increase of fire plume tilt angles with the fire sizes. In addition, CFD also predicted that the fire plume tilt angle decreases with the increase of compartment aspect ratio.

It can be observed in Table 2 that the plume in compartment **A** has the highest deflection angle from the vertical. In contrast, the plume in compartment **D** has the smallest deflection angle from the vertical. The deflection angles vary from 75° to 56° in compartment **A** to compartment **D** at 3.0 kW. The deflection angles at 15.0 kW fire vary from 87° to 60°. The overall comparison shows that at specific compartment and fire size, the predicted plume tilts angle was slightly lesser than the experimental results.

Table 2: Predicted fire plume tilt angles.

Fire Size	Compartment A		Compartment B		Compartment D	
(kW)	Measured	Predicted	Measured	Predicted	Measured	Predicted
3.0	75°	75°	70°	65°	60°	56°
15.0	79°	87°	73°	65°	70°	60°

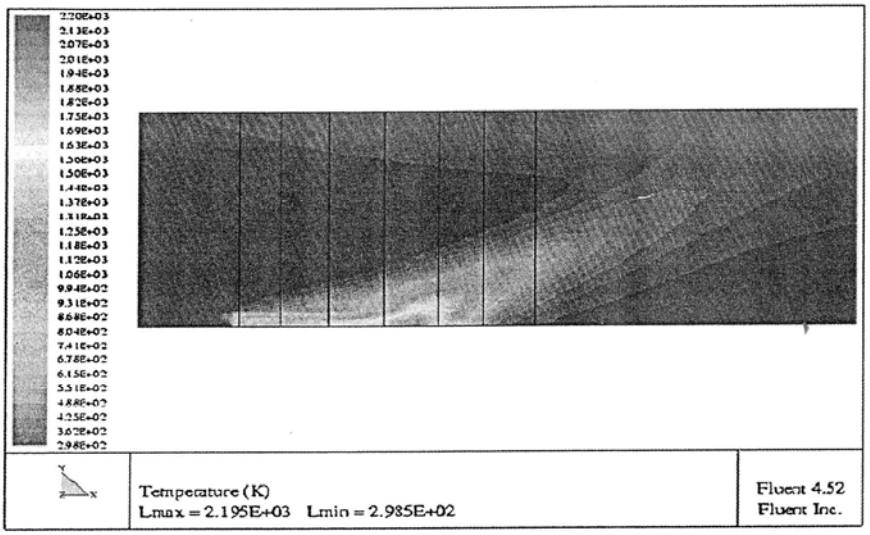

Fig. 7a: Temperature distribution in compartment B for 3.0 kW fire.

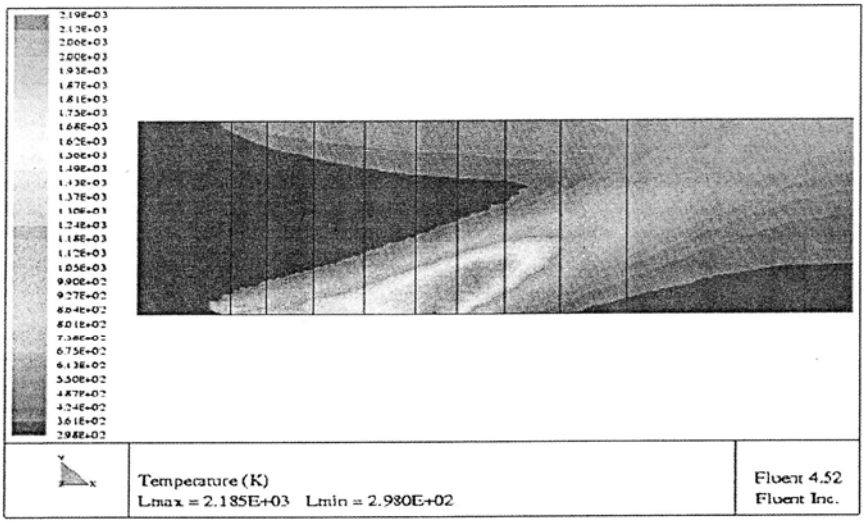

Fig. 7b: Temperature distribution in compartment B for 7.50 kW fire.

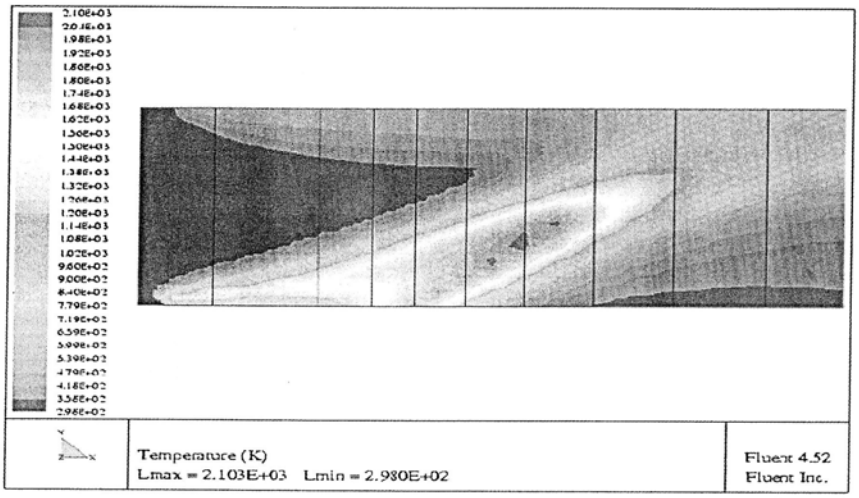

Fig. 7c: Temperature distribution in compartment B for 15.0 kW fire.

5. CONCLUSION

The dynamic fire in four compartments has been studied by performing both experimental and Computational Fluid Dynamic modeling. The results show that the distribution of the fire plume inside the compartment depends greatly on the interaction between the fire with the ventilation flow and compartment walls.

The compartment walls also gave significant effect on the distribution of the fire plume. When the compartment is narrow, the flame has to elongate further downstream for the air entrainment due to the limited spaces at both sides of the fire. In contrast, when the compartment is wide, there are greater tendencies for entrainment from both sides due to more spaces available. Therefore, it would be expected that the local acceleration near the fire seat is greater when the compartment is wide. As a result, the fire would have less deflection angle from the vertical.

Computational Fluid Dynamics was able to predict the behavior of compartment fires similar to the experimental works. The utility of CFD will be the driving force to study fire phenomenon since this technique consume less time and enables us to model fire in a complex geometry.

NOMENCLATURE

k	the turbulence energy m^2s^{-2}
ε	the rate of viscous dissipation of turbulence energy m^2s^{-3}
μ	the turbulence effective viscosity $kgm^{-1}s^{-1}$
C_1	constant
C_2	constant
C_μ	constant
$C_{3\varepsilon}$	constant
σ_k	constant
σ_ε	constant

REFERENCES

[1] A.J.M, Heselden, "Studies of Fire and Smoke Behavior Relevant to Tunnel", Building Research Establishment, CP66/1978, pp 1-14, 1978.

[2] M.Z, Abu Bakar, "Control of Smoke Flow in Tunnel Fires" PhD Thesis, University of Sheffield, UK, 1999.

[3] Y.,Wu and M.Z.A.Bakar, "Control Smoke Flow in Tunnel Fires Using Longitudinal Ventilation Systems – A Study of The Critical Velocity", Fire Safety Journal, Vol 35, page 363-390, 2000 John Wiley, UK.

[4] G.T, Atkinson and Y. Wu, "Smoke Control in Sloping Tunnel" Fire Safety Journal, Vol 27, pp 322-335, 1996.

[5] D.D, Drysdale, " An Introduction to Fire Dynamic", 1985, Wiley and Son.

[6] BS 1042: Section 1:1 "Measurement of Fluid Flow in Closed Conduit", 1989.

[7] B.F. Magnussen and B.H. Hjertager, "On mathematical modelling of turbulent combustion with special emphasis on soot formation and combustion", Proceedings of 16th International Symposium on Combustion, The Combustion Institute, pg 719-729, 1976.

[8] B.E.Launder and D.B. Spalding, "The numerical computation of turbulent flows", Journal Computational Methods Appl Mech Engineering, Vol 3 pg 269-289, 1974.

[9] M. Ljuboja and W. Rodi, "Calculation of turbulent wall jets with an algebraic Reynolds stress models", Journal Fluids Enging Trans, ASME, 1980.

[10] P.J. Woodburn and R.E Britter "CFD Simulations of a tunnel fire- Part 1", Fire Safety Journal, Vol 26, pg 35-62, 1996.

[11] P.J. Woodburn and R.E Britter, "CFD Simulations of a tunnel fire- Part 2", Fire Safety Journal, Vol 26, pg 62-90, 1996.

[12] B.J. Mc Caffrey, "Purely buoyant diffusion flames: some experimental results", National Bureau of Standards, NBSIR 79-1910, 1979.